Toughening of Poly(L-lactide) by Melt Blending with Rubbers

Sachiko Ishida,[1] Reiko Nagasaki,[2] Keisuke Chino,[2] Tungalag Dong,[1] Yoshio Inoue[1]

[1]*Tokyo Institute of Technology, 4259-B55 Nagatuta, Midori-ku, Yokohama 226-8501, Japan*
[2]*Research and Development Center, Yokohama Rubber Company, Limited, 2-1 Oiwake, Hiratsuka, Kanagawa 254-8601, Japan*

Received 28 July 2008; accepted 25 January 2009
DOI 10.1002/app.30134
Published online 19 March 2009 in Wiley InterScience (www.interscience.wiley.com).

ABSTRACT: Poly(L-lactide) (PLA) was melt-blended with four rubber components—ethylene–propylene copolymer, ethylene–acrylic rubber, acrylonitrile–butadiene rubber (NBR), and isoprene rubber (IR)—in an effort to toughen PLA. All the blend samples exhibited distinct phase separation. Amorphous PLA constituted a topologically continuous matrix in which the rubber particles were dispersed. According to Izod impact testing, toughening was achieved only when PLA was blended with NBR, which showed the smallest particle size in its blend samples. In agreement with the morphological analysis, the value of the interfacial tension between the PLA phase and the NBR phase was the lowest, and this suggested that rubber with a high polarity was more suitable for toughening PLA. Under the tensile stress conditions for NBR and IR blend samples, these rubbers displayed no crosslinking and showed a high ability to induce plastic deformation before the break as well as high elongation properties; this suggested that the intrinsic mobility of the rubber was important for the dissipation of the breaking energy. © 2009 Wiley Periodicals, Inc. J Appl Polym Sci 113: 558–566, 2009

Key words: biodegradable; interfaces; mechanical properties; plastics; rubber

INTRODUCTION

Poly(L-lactide) (PLA) is well known as a biocompatible and biodegradable thermoplastic, and it is producible from renewable carbon sources such as starch and sugar. Recently, PLA has attracted much attention because of its high biocompatibility and good biodegradability and mechanical properties.[1–4] Therefore, PLA has great potential as a new general-purpose resin and as an alternative to petroleum-based plastic materials. In fact, PLA and its copolymers have been used for biomedical applications, such as drug delivery systems, implant materials for bone fixation, and surgery. However, with a glass-transition temperature ranging from 55 to 65°C, PLA is too stiff and brittle for room-temperature applications, and this brittleness is a major drawback for expanding its applications as a common plastic material.

In analogy to other brittle materials, PLA can be toughened through blending with other polymers. Although numerous attempts have been made to toughen PLA through blending, the focus has typically been on biomedical applications, so biocompatible polymers such as poly(vinyl alcohol),[5,6] poly(ε-caprolactone),[7] poly(ethylene glycol) (PEG),[8–11] polyhydroxyalkanoate, and poly(butylene succinate)[12] have generally been used as second-phase polymers. Before these blends become perfect materials, however, some problems need to be solved. For example, the PLA/PEG blend exhibits the desired mechanical properties, but there is serious evidence that this blend is not stable and that the attractive mechanical properties are lost over time.[13] The biodegradable aspects of PLA are important, but the fact that it is derived from renewable resources makes it even more attractive. Because currently the problem of limited petroleum resources is getting more and more acute, there is a pressing need for an alterative to petroleum-based plastics. Altogether, the mechanical properties of PLA blends need to be improved further.

Some properties of polymer blends depend not only on the chemical composition of the blend but also on the compatibility or miscibility of the components. However, most polymer blend systems are immiscible. The impact strength of a two-phase polymer system is generally influenced by several morphological parameters, such as the particle size, particle size distribution, particle volume fraction, particle configuration in the matrix, and matrix ligament thickness (surface-to-surface interparticle distance). However, some of the morphological parameters are interrelated.

Correspondence to: Y. Inoue (inoue.y.af@m.titech.ac.jp).

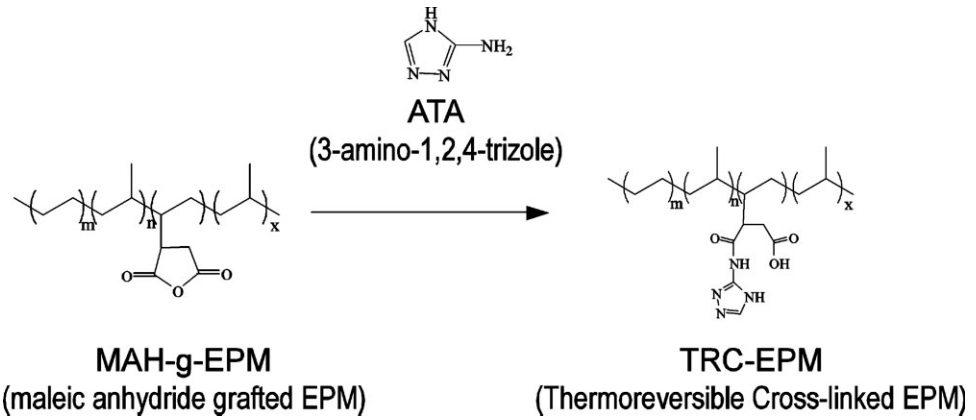

Figure 1 Schematic pathway for the synthesis of thermoreversibly crosslinked EPM.

Rubber has been used as a second-phase polymer for toughening brittle materials, such as epoxy,[14] polypropylene,[15–17] poly(methyl methacrylate),[18–21] polystyrene,[22,23] and polyamide.[24,25] In general, the spherical rubber particles act as stress concentrators, initiating and terminating crazes in the brittle polymer matrices, which are responsible for the enhanced fracture energy absorption.[26–28] Therefore, in these rubber-blended polymer systems, the relationships between the impact strength of the blends and the morphological parameters have been investigated in detail.[29–33]

To date, however, the miscibility, phase behavior, and mechanical properties of PLA/rubber blends have been less well investigated. In this study, a novel PLA material created through blending with rubber was prepared. For blending rubbers, we chose four kinds of rubbers: ethylene–propylene copolymer (EPM), ethylene–acrylic rubber (AEM), acrylonitrile–butadiene rubber (NBR), and isoprene rubber (IR). Because NBR and IR are not sulfur-crosslinked rubbers and AEM and EPM are thermoreversibly crosslinked rubbers, the reuse of these rubbers as raw materials is possible. In this article, we investigate the mechanical performances and morphologies of PLA blended with different types of rubbers, and the effects of each rubber's polarity, crosslinking, and blend ratio on the morphology and impact strength are also discussed.

EXPERIMENTAL

Materials

PLA pellets (Lacea H-100; weight-average molecular weight = 116,000) and maleic anhydride grafted EPM (MP0620; maleic anhydride grafted in the proportion of 1.0 wt %) were provided by Mitsui Chemicals, Inc. (Tokyo, Japan). NBR (Nipol 1043) and IR (Nipol 2200) were produced by Nippon Zeon Co., Ltd. (Tokyo, Japan). Maleic anhydride grafted AEM (AR201; maleic anhydride grafted in the proportion of 1.0 wt %) was provided by Du Pont–Mitsui Polychemicals Co., Ltd. (Tokyo, Japan). PLA, NBR, and IR were used without further purification. 3-Amino-1,2,4-triazole (ATA), purchased from Nippon Carbide Industries Co., Inc. (Tokyo, Japan), was used for the synthesis of thermoreversibly crosslinked AEM and EPM.

AEM and EPM rubber compounds were thermoreversibly crosslinked as shown in Figure 1. The addition of the active hydrogen compound, that is, ATA, to maleic anhydride grafted rubber was the step used to generate a hydrogen-bonding moiety in the rubber phase, creating thermoreversibly crosslinked rubbers.[34–36]

Blend preparation

To study the effect of blending various rubber components into PLA on the mechanical properties and morphologies, it was necessary to make comparisons with a constant rubber content. The concentration of the rubbers in the blends was fixed at 10 or 20 wt %. The blends were prepared by melt compounding for 30 min at 200°C with a PBV-0.3 desktop kneader (Irie Shokai Co., Ltd., Japan) and compression molding for 3 min at 200°C under 5 MPa. The samples were then cooled to room temperature with circulating water.

Differential scanning calorimetry (DSC)

The DSC data for the pure PLA and the PLA/rubber blend samples were recorded on a Seiko Exstar 6000 system equipped with a DSC 220U (Seiko Instruments Co., Tokyo, Japan). A sample (3–5 mg) in an aluminum pan was heated from 25 to 200°C at a heating rate of 10°C/min (the first heating scan). The melting temperature was taken as the peak top of the DSC endotherm. The samples were melted in the DSC apparatus at 200°C for 2 min, quenched to

−80°C with liquid nitrogen, and then reheated up to 200°C at a heating rate of 10°C/min (the second heating scan). The glass-transition temperature was taken as the inflection point in the jump of the heat capacity in the second heating scan as the summit of the peak of the differentiated DSC curve.

Characterization of the blend morphology

The morphology of the pure PLA and the PLA/rubber blends was investigated with scanning electron microscope (SEM; JSM-5200, JEOL, Tokyo, Japan). The samples were immersed and kept in liquid nitrogen for 30 min and then were broken cryogenically. After sputter coating with a thin film of gold on the fractured surface with an Eiko IB-3 ion coater (Eiko Co., Kobe, Japan), the specimens were examined.

Izod impact test

Izod impact tests were performed according to JIS-K7110. The specimens were 10 mm thick and 4.0 mm wide. To study the fracture mechanism of the blends, the Izod-fractured surface was observed with SEM.

Tensile testing

Tensile properties of the blend sample were investigated by tensile testing with an EZ tester (Shimadzu Co., Ltd., Tokyo, Japan). The crosshead speed was 2 mm/min. Five specimens were tested for each set of samples, and the mean value and the standard deviation were calculated.

Contact-angle measurements

The contact angle was measured by the sessile drop technique with a contact-angle goniometer (CA-X, Kyowa Interface Science Co., Ltd., Tokyo, Japan). To calculate the solid surface free energy values of the pure components, we used two different liquids whose values of the dispersion force component of the liquid surface free energy ($\sigma_L{}^d$) and the polar force component of the liquid surface free energy ($\sigma_L{}^p$) were known, that is, water ($\sigma_L{}^d = 21.8$ and $\sigma_L{}^p = 51.0$ dyn/cm) and formamide ($\sigma_L{}^d = 39.5$ and $\sigma_L{}^p = 18.7$ dyn/cm).[37] At first, a small drop of each liquid was placed on the test surface and was allowed to equilibrate for about 60 s, and then the contact angle was measured.

PLA and rubber sample films were prepared by compression molding between Teflon sheets for 3 min under a pressure of 5 MPa with a Mini Test Press 10 laboratory press (Toyoseiki Co., Japan) at the following temperatures: 200°C for PLA, 80°C for NBR, 70°C for IR, 120°C for AEM, and 170°C for EPM.

Data analysis: Estimation of the interfacial tension between PLA and rubber

The interfacial tensions between the PLA phase and rubber phase in the PLA/rubber blend samples were calculated with the solid surface free energies of the pure components determined by contact-angle measurements. Young's equation for the contact of a liquid with a solid is

$$\sigma_{LV} \cdot \cos\theta = \sigma_{SV} - \sigma_{SL} \quad (1)$$

where θ is the contact angle and σ_{LV}, σ_{SV}, and σ_{SL} are the free energies of the liquid and solid against their saturated vapor and of the interface between the liquid and solid, respectively.[38] Approaches used to obtain the value of the solid surface free energy from the contact-angle data are essentially ways to calculate the unknown interfacial tension between the polymer solid and the test liquid. According to Owens and Wendt, this equation takes the following form:[38,39]

$$\sigma_{SL} = \sigma_{SV} + \sigma_{LV} - 2(\sigma_{LV}^d \sigma_{SV}^d)^{1/2} - 2(\sigma_{LV}^d \sigma_{SV}^d)^{1/2} \quad (2)$$

where σ^d is the dispersion force component and σ^p is the polar force component of the surface free energy ($\sigma = \sigma^d + \sigma^p$). Through the measurement of the contact angles of two different liquids against a solid, simultaneous equations can be obtained that can be solved for $\sigma_S{}^d$ and σ_S^p.

The values of these surface free energy parameters can be used to estimate the blend interfacial tension with the appropriate methods. One of the simplest methods is Antonoff's rule,[40,41] which relates the polymer surface energy (σ_i and σ_j) to the interfacial tension (σ_{ij}):

$$\sigma_{ij} = |\sigma_i - \sigma_j| \quad (3)$$

Antonoff's rule has been found to provide an acceptable estimate of the interfacial energy for some polymer blends,[14,42] so we determined the interfacial tensions between the PLA phase and rubbers phase using this equation.

RESULTS AND DISCUSSION

DSC analysis

Figure 2(a) shows the DSC thermograms from the first heating scan for the pure PLA and PLA/rubber blend samples. These samples were prepared by compression molding at 200°C and subsequent rapid cooling. In each thermogram, there was a very large cold crystallization exotherm, the area of which was

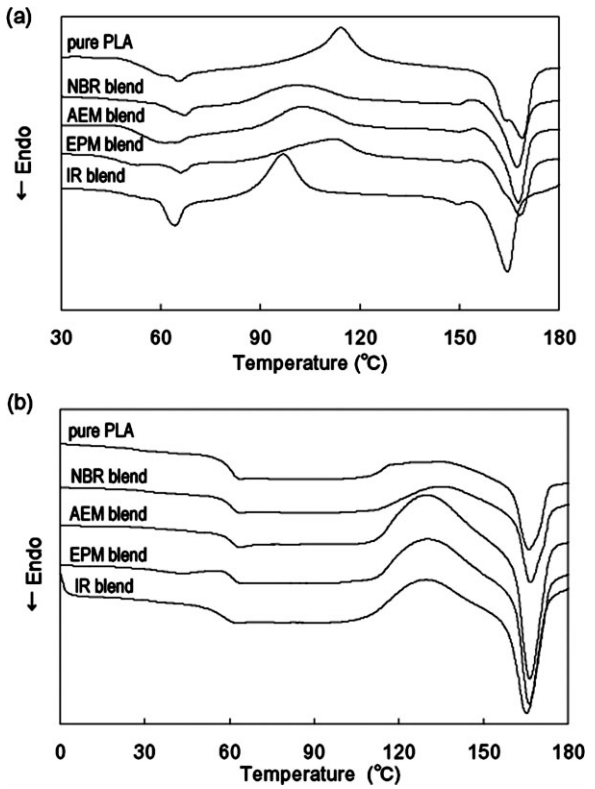

Figure 2 DSC curves of pure PLA and PLA/rubber blends: (a) first heating scan and (b) second heating scan.

quite similar to that of the melting endotherm; this suggested that the PLA component in each blend was almost in the amorphous state. The broad halo observed in wide-angle X-ray scattering patterns (data not shown) also confirmed this DSC result. In the first heating scan, the pure PLA had melting temperatures of approximately 164 and 169°C and a crystallization exotherm starting at about 90°C and ending at about 140°C. As shown in Figure 2(b), PLA in the blend samples exhibited the same glass-transition temperature as pure PLA, that is, about 60°C; this suggested that the PLA–rubber blend systems were immiscible.

Blend morphology

Figure 3 presents SEM micrographs of cryofractured surfaces. As expected from the DSC analysis, each blend showed a particle-dispersed morphology caused by phase separation. That is, rubber particles in the PLA matrix and smooth, distinct particle interfaces, indicating poor interfacial adhesion, were observed. Among the four rubber blend samples, the particle size of the NBR blend was the smallest [3–4 μm; Fig. 3(a)], and those of the AEM [Fig. 3(b)] and IR blends [Fig. 3(c)] were almost 4 and 6 times larger than those of the NBR blend, respectively; the EPM blend exhibited some particle flocculation, producing a large dispersed phase [Fig. 3(d)].

The reason for such morphological features underlies the rheological behavior of the two individual components. The breakup of the particles is governed by viscous forces and interfacial forces.[24] Taylor[43,44] modeled the drop size for a Newtonian fluid in a simple shear field with the viscosity ratio (η_r = dispersed phase viscosity/matrix phase viscosity) and the capillary number [$Ca = \gamma\eta_m D/(2\sigma)$, where γ is the shear rate, η_m is the matrix viscosity, σ is the

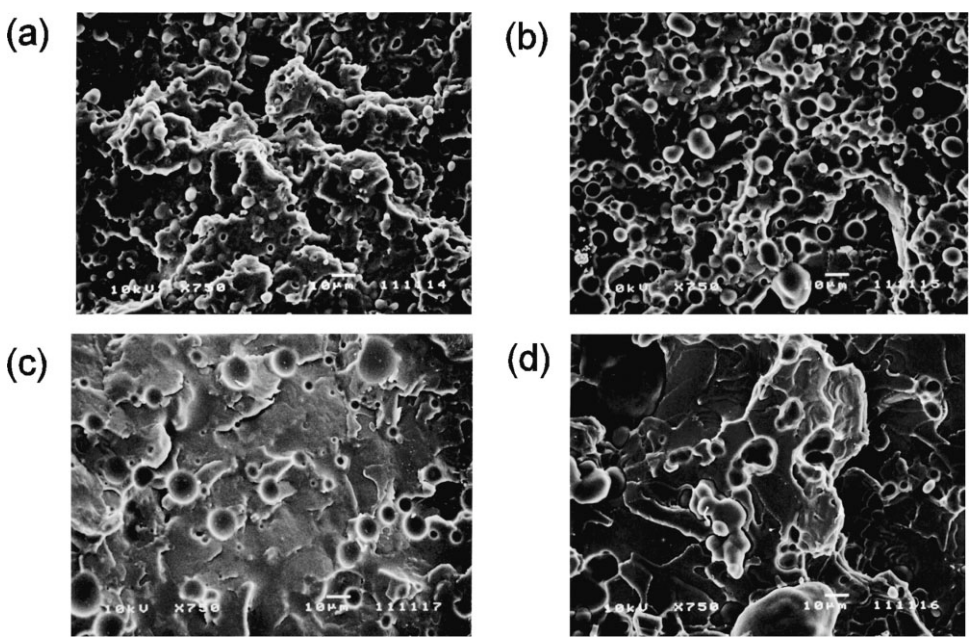

Figure 3 SEM micrographs of freeze-fractured surfaces of 10 wt % (a) NBR, (b) AEM, (c) IR, and (d) EPM blends.

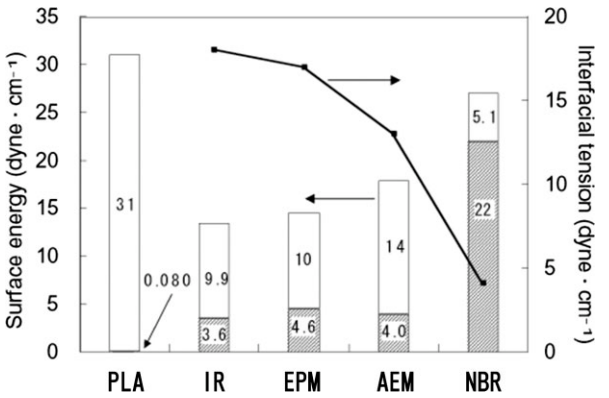

Figure 4 Surface energy and interfacial tension between PLA and rubbers.

interfacial tension between the dispersed phase and the matrix phase, and D is the maximum drop size]. By balancing the interfacial forces and the shear forces, Taylor obtained a relationship for a value of D that would be stable:

$$D = \frac{4\sigma(\eta_r + 1)}{\gamma\eta_m\left(\frac{19}{4}\eta_r + 4\right)} \quad (4)$$

Under processing conditions, the values of γ and η_m were equal in the four rubber blend samples. Then, the rubber particle size could be affected by the values of η_r and σ. As understood from eq. (4), the particle size of the dispersed rubber phase is more influenced by the value of σ than by the value of η_r. Therefore, we evaluated the effect of the interfacial tensions between the PLA and rubbers. However, there is no method available for measuring directly the interfacial tension between PLA and rubbers in their blends. This is mainly due to the absence of suitable methods for measuring the interfacial tension of high-molecular-weight/high-viscosity blends. Therefore, we estimated the values of the interfacial tensions via contact-angle measurements at room temperature (see the Data Analysis section).

In Figure 4, the bar graphs present the surface free energies, which consist of dispersion and polar components, calculated from contact-angle measurements. Then, a line graph exhibits the interfacial tensions between the PLA and rubbers derived from the values of the surface free energies with eq. (2). As for pure PLA, the values of σ_S^d (31 dyn/cm) and σ_S^p (0.080 dyn/cm) were slightly smaller than the literature values (39.6 $\pm$ 1.7 and 3.9 dyn/cm, respectively,[45] and 36.0 and 4.24, 36.6 and 0, and 35.9 and 0 dyn/cm, respectively[46]). It was thought that this disagreement with the literature value might be caused by the difference in the roughness of the surfaces of the sample films prepared. From these measured values of the surface free energies, we calculated the interfacial tension between PLA and rubber. As shown in Figure 4, the interfacial tension between PLA and rubber decreased in the order of IR > EPM > AEM > NBR. This inclination is consistent with the blend morphology. In other words, if the interfacial tension is low, the repulsion of chain segments in the presence of incompatible chain segments due to the interaction energy is low; therefore, the rubber phase disperses well, and the particle size decreases. Analogous reductions of the particle size of dispersed-phase polymers were found in plasticized PLA and other polymer blends when they were compounded with a copolymer or coupling agent.[22,47]

The surface free energies of rubbers seem to become high when the polarity becomes high; that is, NBR with 29% cyano groups exhibited the highest surface energy. Because PLA has hydroxyl groups, it is thought that the polar segments of rubbers might enhance the compatibility and reduce the repulsion forces under melt-blending conditions.

Izod impact strength

Figure 5 shows SEM micrographs of the fractured surfaces, which were formed during Izod impact tests at room temperature. Two phases can be seen clearly, and in the fracture process, many rubber particles were pulled out from the PLA matrix, with large voids thereby being created. It was suggested that the fracture crack ran along the interface between the PLA matrix and the rubber particles.

The Izod impact strength is summarized in Figure 6. Only the NBR blend showed higher impact strength than pure PLA. The improvement in the impact strength is most likely attributable to the smaller rubber particle size in the PLA matrix. In other words, the NBR blend possessed the smallest rubber particle size (3–4 μm) and exhibited high efficiency in toughening PLA; subsequently, the impact strength decreased in the order of increasing rubber particle size in the blends. In fact, such a correlation has been frequently observed for other rubber-modified polymers.[48] As shown in Figure 6, the impact strength of the 20 wt % EPM blend increased in comparison with that of the 10 wt % blend. Figure 7 presents an SEM micrograph of the cryofractured 20 wt % EPM blend. The 20 wt % EPM blend possessed a somewhat flocculated morphology, but the degree of flocculation was less severe than that of the 10 wt % blend, which exhibited a large dispersed rubber phase. Compared to the 10 wt % EPM blend, the 20 wt % EPM blend had more small rubber particles. To address the reason that the blend morphology was so different between the 10 and 20 wt % EPM blends, we have to consider the coalescent effect. There are some reports about the composition effect on the final particle size in immiscible polymer

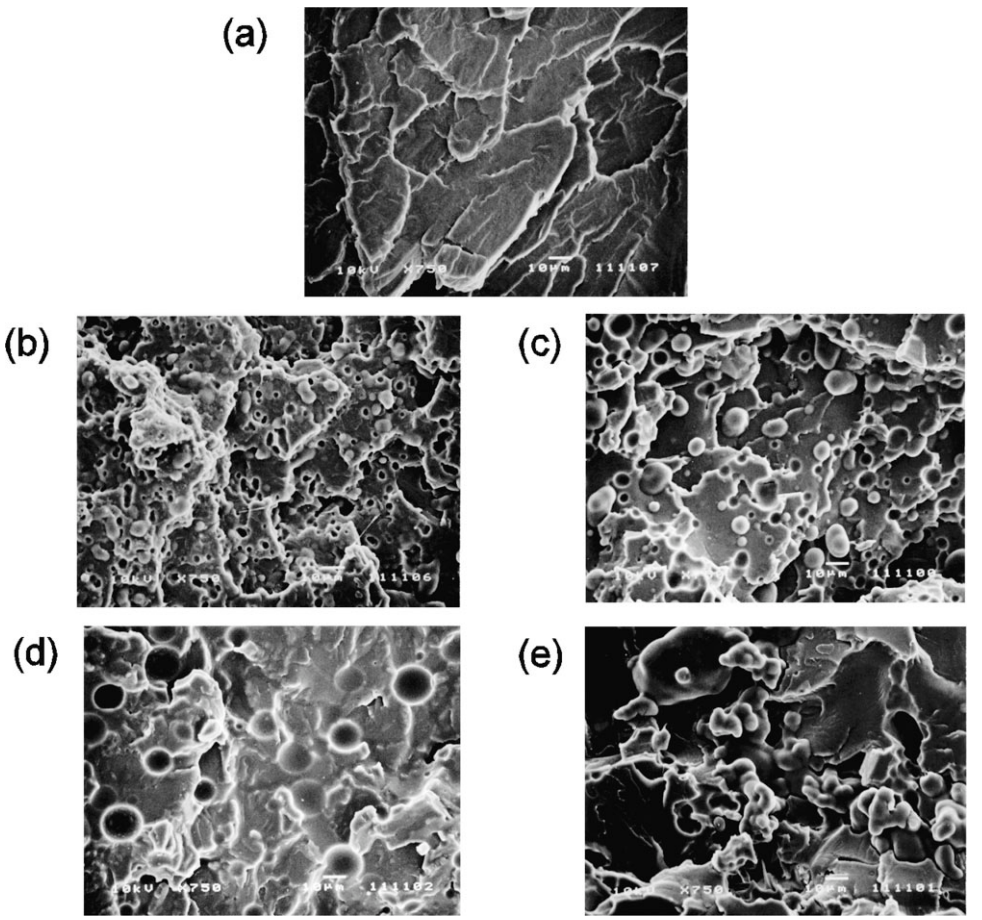

Figure 5 SEM micrographs of Izod-impact-fractured surfaces of (a) pure PLA and 10 wt % (b) NBR, (c) AEM, (d) IR, and (e) EPM blends.

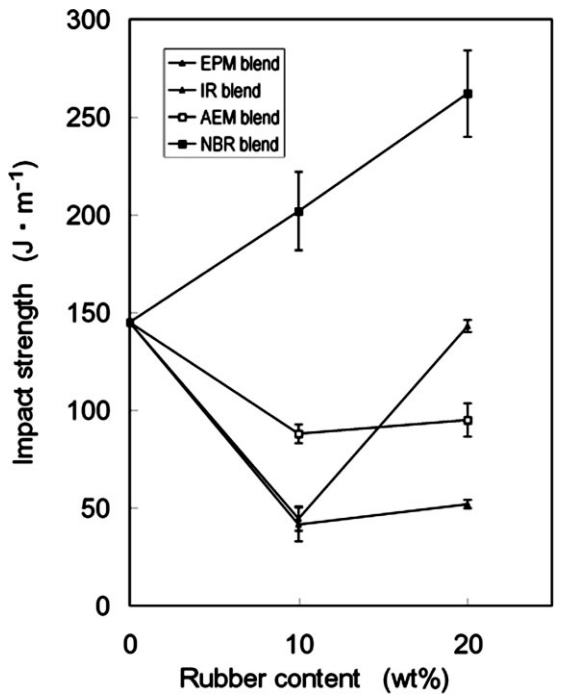

Figure 6 Impact strength of pure PLA and PLA/rubber blends. Error bars represent one standard deviation obtained from the testing of five specimens.

blend systems. Sundararaj and Macosko[49] reported that the particle size distribution broadens at higher concentrations because breakup and coalescence are occurring concurrently during blending at higher concentrations. This fact can partially account for the

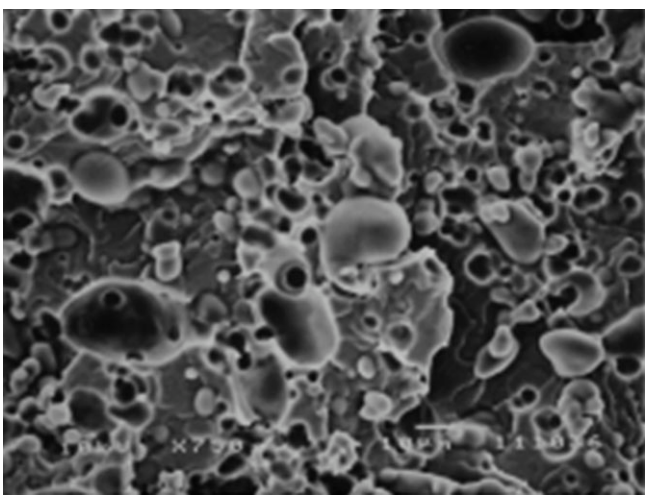

Figure 7 SEM micrograph of the Izod-fractured surface of the 20 wt % EPM blend.

morphology difference of the EPM blends. Thus, the 20 wt % EPM blend had a broader particle size distribution, and the EPM rubber composition was twice that in the 10 wt % blend, so many small particles could be observed. Although the cause of the morphology difference between the 10 and 20 wt % EPM blends is not completely clear, this fact also proves that the rubber particle size considerably affected the impact strength.

A brittle–ductile transition has been observed in many rubber-toughened plastics,[13,30,50] in other polymer blends,[16,27] and in inorganic-particle-modified polymers.[51,52] This transition is very sharp, and the critical factors that determine the onset of the brittle–ductile transition, such as the rubber particle size and spatial distribution, interfacial adhesion between PLA and rubber, rubber blend ratio, and matrix ligament thickness, have been investigated. Wu[53,54] suggested that the matrix ligament thickness is the primary controlling factor for rubber toughening in polymer blends. The matrix ligament thickness is defined as the surface-to-surface dispersed-phase interparticle distance. Wu indicated that if the average matrix ligament thickness is below the critical value, then the blend will be tough; if the average matrix ligament thickness is above the critical value, the blend will be brittle. On the basis of an investigation of PLA/linear low-density polyethylene blends with notched Izod impact testing, Anderson et al.[47] reported that the critical matrix ligament thickness of PLA was approximately 1.0 μm and that ductile blend samples exhibited impact resistance about 40 times as high as that of pure PLA. Similarly to Anderson et al.'s report, for other rubber-modified polymers in the ductile state, the impact strength increased. As shown in Figure 5, however, the matrix ligament thickness of the PLA/rubber blend was more than 1.0 μm; the highest impact strength was about 1.8 times the impact strength of pure PLA. Although the critical value in the notched Izod impact testing may not be directly compared with that in the Izod impact testing, it was thought that the NBR blend was not completely ductile. Therefore, the NBR blend could become tougher if the phase-separation morphology became more suitable (i.e., thinner ligament thickness).

Other rubber blends exhibited more brittleness than pure PLA. It was thought that larger rubber particles promoted crack propagation by exfoliation at the interface between the PLA matrix and the rubber particles, which resulted in the brittleness.

Tensile testing

The tensile properties are shown in Figure 8. The tensile modulus and tensile strength of the PLA/rubber blends decreased by about 39 and 52%, respectively, in comparison with those of pure PLA. These properties of the blends were not significantly affected by the type of rubber. For the EPM blend and the AEM blend, the elongation decreased by 61%, but that of the NBR blend increased slightly, and that of the IR blend increased 2 times or more. Because there was no significant difference among the four blend samples in the tensile modulus and tensile strength, it is believed that the difference in elongation was caused by that in the areas of the plastic deformation zone, where the materials showed whitening. This explanation is confirmed by the fact that the IR and NBR blend samples showed larger plastic deformation zones near the fracture flank in comparison with the AEM and EPM blends. As AEM and EPM are crosslinked rubbers with thermoreversible hydrogen bonds but IR and NBR are not, the mobility of the chains is high, and it is thought that the relief for tensile stress can easily

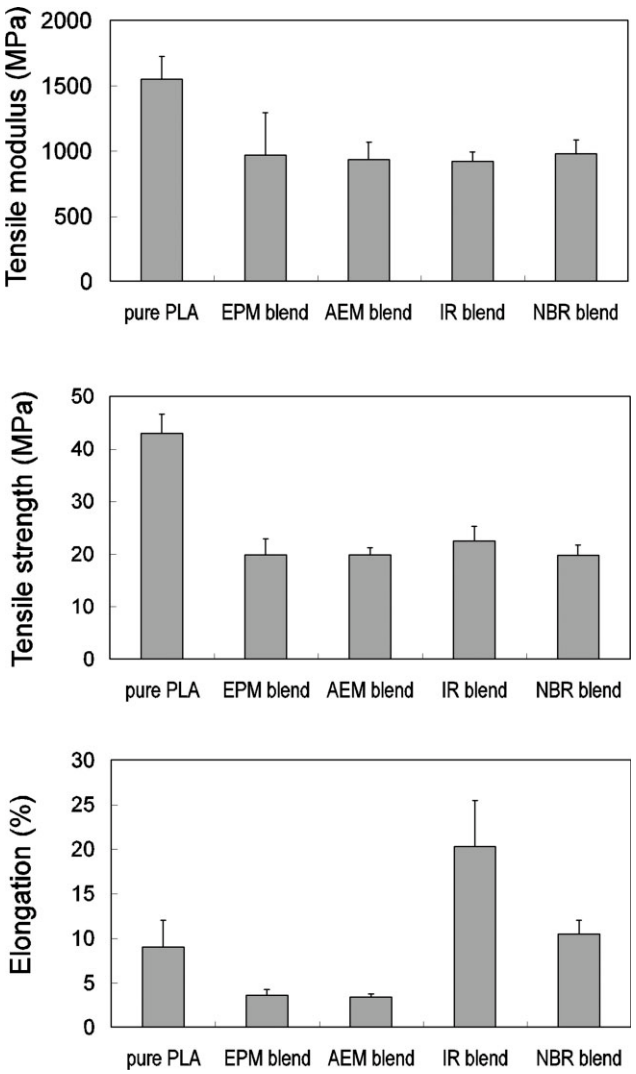

Figure 8 Tensile modulus, tensile strength, and elongation of pure PLA and PLA/rubber blends.

occur. These characteristics of IR and NBR allow the rubber particles to cavitate under the tensile stress conditions. This cavitation, in turn, allows unconstrained plastic flow of the matrix ligaments before the fatal crack run, resulting in the high elongation properties.

CONCLUSIONS

By melt-blending rubber components, we were able to achieve at most 1.8-fold toughening of amorphous PLA. In this study, the distributed rubber particle size seriously affected the toughness of PLA. The NBR blend possessed the smallest rubber particle size (3–4 μm) and exhibited a 2 times higher value of the impact strength in comparison with PLA; subsequently, the impact strength decreased in the order of increases in the rubber particle size in the blends. The reason for such morphological features underlies the rheological behavior and especially the interfacial tension between the PLA matrix and dispersed rubber particles. NBR with 29% cyano groups exhibited the highest surface energy and the lowest interfacial tension with PLA. This favorable interaction seems to result in the well-dispersed rubber phase and the smallest rubber particle size. We can see some possibility of the final blend morphology being predicted by the interfacial tension between PLA and rubber and even by the rubber's polarity estimated from the chemical structure. This is useful for the first step of selecting a rubber to be blended with PLA.

However, PLA in the NBR blend was not in a completely ductile state. It is thought that the impact strength of an NBR blend could increase if the NBR particle size becomes smaller. For the achievement of a good dispersed morphology, the blend preparation method must be improved (e.g., the addition of block copolymers and compatibilizers).

The results obtained from the tensile tests showed that the NBR and IR blends possessed a high ability to induce plastic deformation before the break as well as high elongation properties. This property seems to come from the absence of rubber crosslinks. Therefore, for the tensile properties, the intrinsic mobility of the rubber is important, and high mobility of the rubber chains promotes plastic flow.

Because the impact strength is controlled by many parameters and some of them are interrelated, elaborative experiments that can divide each effect need to be performed. Further work should yield some fascinating surprises and new insights.

References

1. Reeve, M. S.; McCathy, S. P.; Downey, M. J.; Gross, R. A. Macromolecules 1994, 27, 825.
2. Tsuji, H.; Miyauchi, S. Polymer 2001, 42, 4463.
3. Jacobsen, S.; Fritz, H. G. Polym Eng Sci 1999, 39, 1303.
4. Jacobsen, S.; Degee, P. H.; Fritz, H. G.; Dubois, P. H.; Jerome, R. Polym Eng Sci 1999, 39, 1311.
5. Gajria, A. M.; Dave, V.; Gross, R. A.; McCarthy, S. P. Polymer 1996, 37, 437.
6. Park, J. W.; Im, S. S. Polymer 2003, 44, 4341.
7. Na, Y. H.; He, Y.; Shuai, X.; Kikkawa, Y.; Doi, Y.; Inoue, Y. Biomacromolecules 2002, 3, 1179.
8. Sheth, M.; Kumar, R. A.; Dave, V.; Gross, R. A.; McCarthy, S. P. J Appl Polym Sci 1997, 66, 1495.
9. Baiardo, M.; Frisoni, G.; Scandola, M.; Rimelen, M.; Lips, D.; Ruffieux, K.; Wintermantel, E. J Appl Polym Sci 2003, 90, 1731.
10. Hu, Y.; Hu, Y. S.; Topolkaraev, V.; Hiltner, A.; Baer, E. Polymer 2003, 44, 5681.
11. Hu, Y.; Hu, Y. S.; Topolkaraev, V.; Hiltner, A.; Baer, E. Polymer 2003, 44, 5711.
12. Park, J. W.; Im, S. S. J Appl Polym Sci 2002, 86, 647.
13. Meredith, J. C.; Amis, E. J. Macromol Chem Phys 2000, 201, 733.
14. Sohn, J. E.; Emerson, J. A. J Appl Polym Sci 1989, 37, 2627.
15. Wang, C. L.; Wang, S. J.; Qi, Z. N. J Polym Sci Part B: Polym Phys 1996, 34, 193.
16. Liu, Z. H.; Zhang, X. D.; Zhu, X. G.; Qi, Z. N.; Wang, F. S. Polymer 1997, 38, 5267.
17. Liu, Z. H.; Li, R. K. Y.; Tjong, S. C.; Qi, Z. N.; Wang, F. S.; Choy, C. L. Polymer 1998, 39, 4433.
18. Memon, N. A.; Muller, R. J Polym Sci Part B: Polym Phys 1997, 36, 2623.
19. Jansen, B. J. P.; Rastogi, S.; Meijer, H. E.; Lemstra, P. J. Macromolecules 1999, 32, 6283.
20. Mina, M. F.; Ania, F.; Balta Calleja, F. J.; Asano, T. J Appl Polym Sci 2004, 91, 205.
21. Cho, K.; Yang, J.; Park, C. E. Polymer 1997, 38, 5161.
22. Mina, M. F.; Haque, M. E.; Balta Calleja, F. J.; Asano, T.; Alam, M. M. J Macromol Sci Phys 2004, 43, 1005.
23. Chuayjuljit, S.; Moolsin, S.; Potiyaraj, P. J Appl Polym Sci 2005, 95, 826.
24. Burgisi, G.; Paternoster, M.; Peduto, N.; Saraceno, A. J Appl Polym Sci 1997, 66, 777.
25. Jose, S.; Thomas, S.; Lievana, E.; Karger-Kocsis, J. J Appl Polym Sci 2005, 95, 1376.
26. Ricco, T.; Pavan, A.; Danusso, F. Polym Eng Sci 1978, 18, 774.
27. Oxborough, R. J.; Bowden, P. B. Philos Mag 1974, 30, 171.
28. Donald, A. M.; Kramer, E. J. J Appl Polym Sci 1982, 27, 3729.
29. Ishiaku, U. S.; Ismail, H.; Mohd Ishak, Z. A. J Appl Polym Sci 1999, 78, 75.
30. Liu, Z. H.; Zhang, X. D.; Zhu, X. G.; Qi, Z. N.; Wang, F. S.; Li, R. K. Y.; Choy, C. L. Polymer 1998, 39, 5027.
31. Liu, Z. H.; Li, R. K. Y.; Tjong, S. C.; Choy, C. L.; Zhu, X. G.; Qi, Z. N.; Wang, F. S. Polymer 1999, 40, 2903.
32. Liu, Z. H.; Zhu, X. G.; Wu, L. X.; Li, Y.; Qi, Z. N.; Choy, C. L.; Wang, F. S. Polymer 1999, 40, 2903.
33. Liu, Z. H.; Zhu, X. G.; Wu, L. X.; Li, Y.; Qi, Z. N.; Choy, C. L.; Wang, F. S. Polymer 2001, 42, 737.
34. Chino, K.; Ashiura, M. Macromolecules 2001, 34, 9201.
35. Chino, K.; Ashimura, M.; Natori, J.; Ikawa, M.; Kawazura, T. Rubber Chem Technol 2002, 75, 713.
36. Chino, K. Kautsch Gummi Kunstst 2006, 59, 158.
37. Kaelble, D. H. J Adhes 1970, 2, 66.
38. Owen, M. J. In Physical Properties of Polymers Handbook; Mark, J. E., Ed.; American Institute of Physics: New York, 1996; p 669.
39. Owens, D. K. J Appl Polym Sci 1969, 13, 1741.
40. Sakurai, T.; Tamai, Y. Ouyou-Kaimen-Kagaku; Asakura-Syoten: Tokyo, 1967; pp 13 and 77.
41. Antonoff, G. N. Ann Phys 1939, 35, 84.
42. Biresaw, G.; Carriere, C. J. J Polym Sci Part B: Polym Phys 2002, 40, 2248.

43. Taylor, G. I. Proc R Soc London A 1932, 138, 41.
44. Taylor, G. I. Proc R Soc London A 1934, 146, 501.
45. Biresaw, G.; Carriere, C. J Polym Sci Part B: Polym Phys 2001, 39, 920.
46. Ringard-Lefebvre, C.; Baszkin, A. Langmuir 1994, 10, 2376.
47. Anderson, K. S.; Lim, S. H.; Hillmyer, M. A. J Appl Polym Sci 2002, 89, 3757.
48. Bartczak, Z.; Argon, A. S.; Cohen, R. E.; Weinberg, M. Polymer 1999, 40, 2331.
49. Sundararaj, U.; Macosko, C. W. Macromolecules 1995, 28, 2647.
50. Grijpma, D. W.; Van Hofslot, R. D. A.; Super, H.; Nijenhuis, A. J.; Pennings, A. J. Polym Eng Sci 1994, 34, 1674.
51. Liu, Z. H.; Zhu, X. Q.; Li, Q.; Qi, Z. N.; Wang, F. S. Polymer 1998, 39, 1863.
52. Bartczak, Z.; Argon, A. S.; Cohen, R. E.; Weinberg, M. Polymer 1999, 40, 2347.
53. Wu, S. Polymer 1985, 26, 1855.
54. Wu, S. J Appl Polym Sci 1988, 35, 549.